Laser Patterning of High-Mass-Loading Graphite Anodes for High-Performance Li-Ion Batteries

Romain Dubey,[a, b] Marcel-David Zwahlen,[c] Yevhen Shynkarenko,[a, b] Sergii Yakunin,[a, b] Axel Fuerst,[c] Maksym V. Kovalenko,*[a, b] and Kostiantyn V. Kravchyk*[a, b]

Given the ongoing efforts to build Li-ion batteries with higher volumetric energy and power densities, the research on enhancing Li-ion transport within compressed high-mass-loading electrodes at fast cycling conditions is imperative. In this work, we show that the rate capability of graphite electrodes with high areal capacity of 4.5 mAh cm^{-2} and density of 1.79 g cm^{-3} (15% of porosity) can be considerably improved by laser patterning, namely by the fabrication of arrays of vertically aligned channels serving as diffusion paths for rapid Li-ion transport. Resultant laser patterned graphite electrodes delivered enhanced volumetric capacity as compared to that of non-patterned electrodes (450 *vs.* 396 mAh cm^{-3} at C/2 rate). The reduction of the total steady-state concentration drop within the graphite electrodes after their patterning was also assessed.

An improvement of the energy density of Li-ion batteries comprising graphite anode coupled with either of LiCoO$_2$, LiFePO$_4$, or LiNi$_x$Co$_y$Mn$_2$O$_2$ cathodes can be achieved only by further reduction of mass contribution of non-active battery components to the overall mass of the battery.[1] In this context, the development of electrodes with maximized areal capacity is imperative. The rate-capability of high-mass-loading electrodes, however, remains a notoriously challenging issue, as a result of slow Li-ion diffusion within thick electrodes leading to severe cell polarization and a significant reduction of the accessible capacity of the electrodes under fast-charge conditions.[2–4] Additionally, the decrease of the potential at the negative graphite electrodes fosters Li plating, the formation of dendrites, and loss of active Li through the accumulation of solid electrolyte interface and dead Li.[5–7]

To circumvent the issues associated with the diffusion-limited rate capability of thick electrodes, a novel electrode architecture has recently been proposed.[8–10] Its central idea is to embed periodically-structured vertical macro-pores/channels in the electrodes in order to decrease through-plane tortuosity and, consequently, enhance the Li-ion diffusion within the electrode (Figure 1a). This follows from the relationship $D_{eff} = \frac{\varepsilon}{\tau_{TP}+\tau_{IP}} D_0$, where D_{eff} is effective diffusivity, D_0 is the electrolyte diffusion coefficient, τ_{TP} is through-plane tortuosity, τ_{IP} is in-plane tortuosity, and ε is electrode porosity.[11] Notably, of all possible strategies for the incorporation of vertically aligned channels such as co-extrusion,[8] magnetic alignment of active material particles[12–14] or laser patterning,[15–20] the latter is probably the most appealing methodology as it can be directly integrated into the existing roll-to-roll manufacturing lines of electrodes without slowing down their production speed.

Herein, we attempted to fabricate a laser-patterned high-mass-loading graphite electrode and further test its rate capability. Although there have been many studies on the patterning of graphite, our work targeted the utilization of ultra-high mass-loading electrodes with an areal capacity of 4.5 mAh cm^{-2}. Previously, the electrochemical performance of patterned graphite anodes was reported only for a much lower areal capacity of 3 mAh cm^{-2}.[15] Moreover, aiming to increase their volumetric capacity, we calendared electrodes to the density of 1.79 g cm^{-3} (denoted as non-patterned electrodes) as compared to the state-of-the-art density of 1.42 g cm^{-3}.[21–22]

In this study, we assessed the pros and cons of laser patterning of highly dense graphite electrodes compared to the non-patterned electrode of the same bulk density. We found that at a C-rate of C/2 or higher, the volumetric capacities of the patterned electrode were higher as compared to non-patterned ones (for instance, 450 *vs.* 396 mAh cm^{-3} for C/2 rate). The lowest volumetric capacities were observed for the electrode with a low overall density of 1.42 g cm^{-3} (denoted as reference electrodes) regardless of the applied current density. The changes of the total steady-state concentration drop of non-patterned, patterned, and reference electrodes were computed for C/20 and 1C rates using the model of Bae et al.[8]

A schematic of studied graphite electrodes is depicted in Figure 1b. Graphite electrodes were prepared by mixing a powder of spheroidized natural graphite, carbon black,

[a] R. Dubey, Dr. Y. Shynkarenko, Dr. S. Yakunin, Prof. M. V. Kovalenko, Dr. K. V. Kravchyk
Laboratory of Inorganic Chemistry
Department of Chemistry and Applied Biosciences, ETH Zürich
Vladimir-Prelog-Weg 1, CH-8093 Zürich, Switzerland
E-mail: mvkovalenko@ethz.ch
        kravchyk@inorg.chem.ethz.ch
[b] R. Dubey, Dr. Y. Shynkarenko, Dr. S. Yakunin, Prof. M. V. Kovalenko, Dr. K. V. Kravchyk
Laboratory for Thin Films and Photovoltaics
Empa – Swiss Federal Laboratories for Materials Science and Technology
Überlandstrasse 129, CH-8600 Dübendorf, Switzerland
[c] M.-D. Zwahlen, Prof. A. Fuerst
Institute for Intelligent Industrial Systems I3S
Berner Fachhochschule
Pestalozzistrasse 20, CH-3400 Burgdorf, Switzerland

Batteries & Supercaps

Communications
doi.org/10.1002/batt.202000253

Chemistry Europe
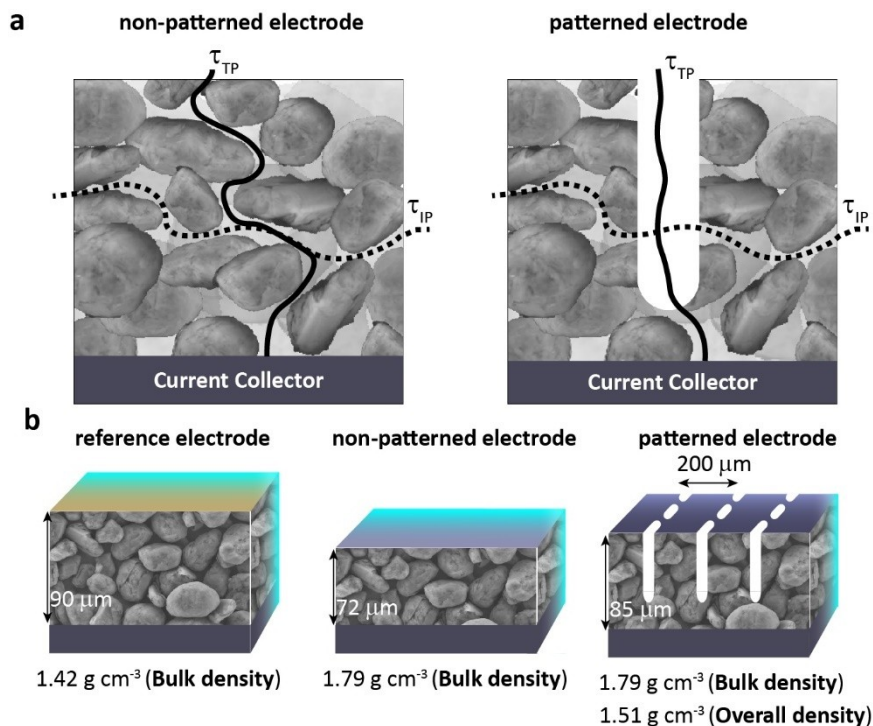European Chemical
Societies Publishing

Figure 1. a) Schematic of in-plane and through-plane paths of Li-ion diffusion in non-patterned and patterned graphite electrodes. b) Schematic of reference, non-patterned, and patterned electrodes used in this study.

carboxymethyl cellulose/styrene-butadiene rubber binders, and water, and the resulting slurries were cast onto a copper foil current collector via doctor-blading. Afterward, graphite electrodes were dried for 12 h at room temperature in an ambient atmosphere, following drying for 12 h at 80 °C under vacuum. Then, the graphite electrodes were calendared to targeted bulk density of *ca.* 1.42 g cm^{-3} and *ca.* 1.79 g cm^{-3}, which corresponds to the porosity of *ca.* 32% and *ca.* 15%, respectively. Cross-sectional SEM images of reference and non-patterned electrodes are shown in Figure S1. Active material loadings were in the range of 10–15 mg cm^{-2} (4.5–5 mAh cm^{-2}).

The basic configuration of the laser patterning setup comprises a 500 mW laser, a chopper, a 2-axis motorized precision positioning stage (xy stage), and a microscope camera, as demonstrated in Figure 2a. The patterning of the electrodes was performed employing picosecond laser pulses (wavelength = 1024 nm) on an area of 1.5×1.5 cm with a channel spacing of 200 μm (Figure 2b).

To examine the surface of graphite anodes after laser patterning, scanning electron microscopy measurements were performed. As follows from Figures 2c–e, after patterning, elongated pore channels with the dimension of 20×80 μm were formed. The average depth of the channels was *ca.* 75 μm (Figure S2). Higher magnification imaging (Figure 2e) demonstrates that laser patterning resulted in through-particle cutting rather than the removal of entire graphite particles. By weighing the electrodes before/after the laser patterning, it was determined that the amount of removed graphite material equals *ca.* 12–15%. The overall density of the patterned

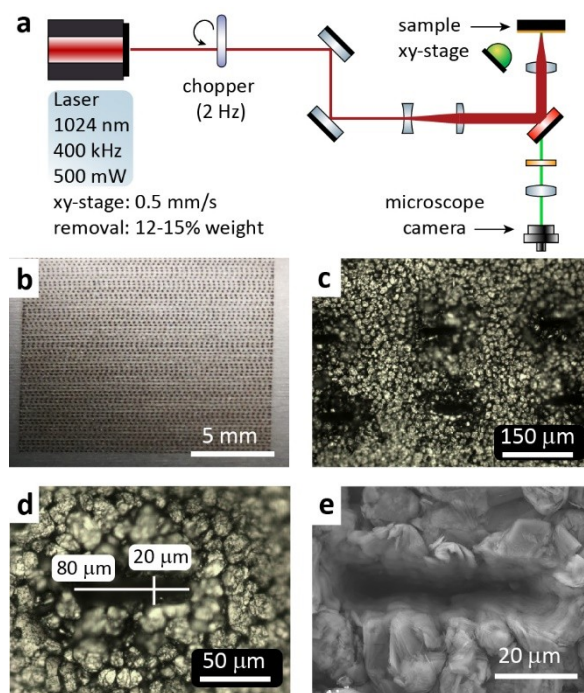graphite was *ca.* 1.51 g cm^{-3}, which corresponds to a porosity of *ca.* 28%.

Figure 2. a) Schematic of the laser patterning setup. b) Photograph of the patterned graphite electrode. Top-view optical (c, d) and SEM (e) images of the holes produced by the laser patterning.

Batteries & Supercaps

Communications
doi.org/10.1002/batt.202000253

Chemistry Europe
European Chemical
Societies Publishing

The electrochemical tests of prepared graphite electrodes were performed using a two-electrode cell configuration. The cell consisted of lithium foil as the counter and the reference electrode, the working graphite electrode, and a glass-fiber separator placed between both electrodes and soaked with lithium electrolyte (1 M $LiPF_6$ in ethylene carbonate/dimethyl carbonate $+3\%$ fluoroethylene carbonate). To evaluate the rate capability of graphite electrodes, cells were charged and discharged within a voltage range of 5 mV–1.5 V at different C rates, employing a constant voltage step at 5 mV. The constant voltage was maintained until the measured current was equal to a 0.05C current value. The cells were first discharged/charged at 0.05C/0.05C rates for 1 cycle, followed by 5 cycles at 0.2C/0.2C, 0.5C/0.2C, 1C/0.2C, 2C/0.2C and 1C/0.2C rates. Afterward, cells were cycled at 0.5C/0.2C rates for 25 cycles. The measured charge storage capacities were normalized to the volume of graphite electrodes.

Figure 3a-c shows the constant current-constant voltage discharge profiles of studied graphite electrodes at discharge C rates of C/20, C/10, C/5, C/2 and 1C. The shape of the voltage curves was characterized by multiple plateaus pointing to the staging mechanism of the Li-ion intercalation in the graphite.[23] Although the initial coulombic efficiency of patterned electrodes (90.8%) was rather similar to the one of reference (91.7%) and non-patterned (89.9%) samples, laser patterning caused

decrease of coulombic efficiency in the following cycles (Figure S5). The latter might originate from substantial increase of the disordered fraction of graphite due to patterning process, as follows from the confocal Raman spectroscopy measurements of a patterned electrode region (Figure S6). Figure 3d summarizes obtained volumetric capacities only under constant current mode. At very low C rates of C/20 and C/5, the non-patterned electrode exhibited higher volumetric capacity in comparison with the patterned electrode (709 and 529 mAh cm^{-3} vs. 610 and 502 mAh cm^{-3}). However, at a higher current density of C/2, 1C, and 2C, as expected, the capacity of the patterned electrode was higher (396, 146, and 46 mAh cm^{-3} vs. 450, 188, and 51 mAh cm^{-3}). The lowest capacity was observed for reference graphite electrodes regardless of the applied current density. These results point out that the highest volumetric capacity of graphite electrodes at fast charging conditions can be reached by reducing the overall porosity of bulk graphite electrode in combination with laser patterning.

To provide further insight into the reasons for the improved performance of the patterned graphite electrodes, we computed the total steady-state concentration drop across studied graphite electrodes, employing the model of Bae et al.[8] This model was previously used to describe the enhancement of the rate capability of $LiCoO_2$ cathode through the fabrication of vertically aligned microchannels. The concept of Bae et al.[8] is
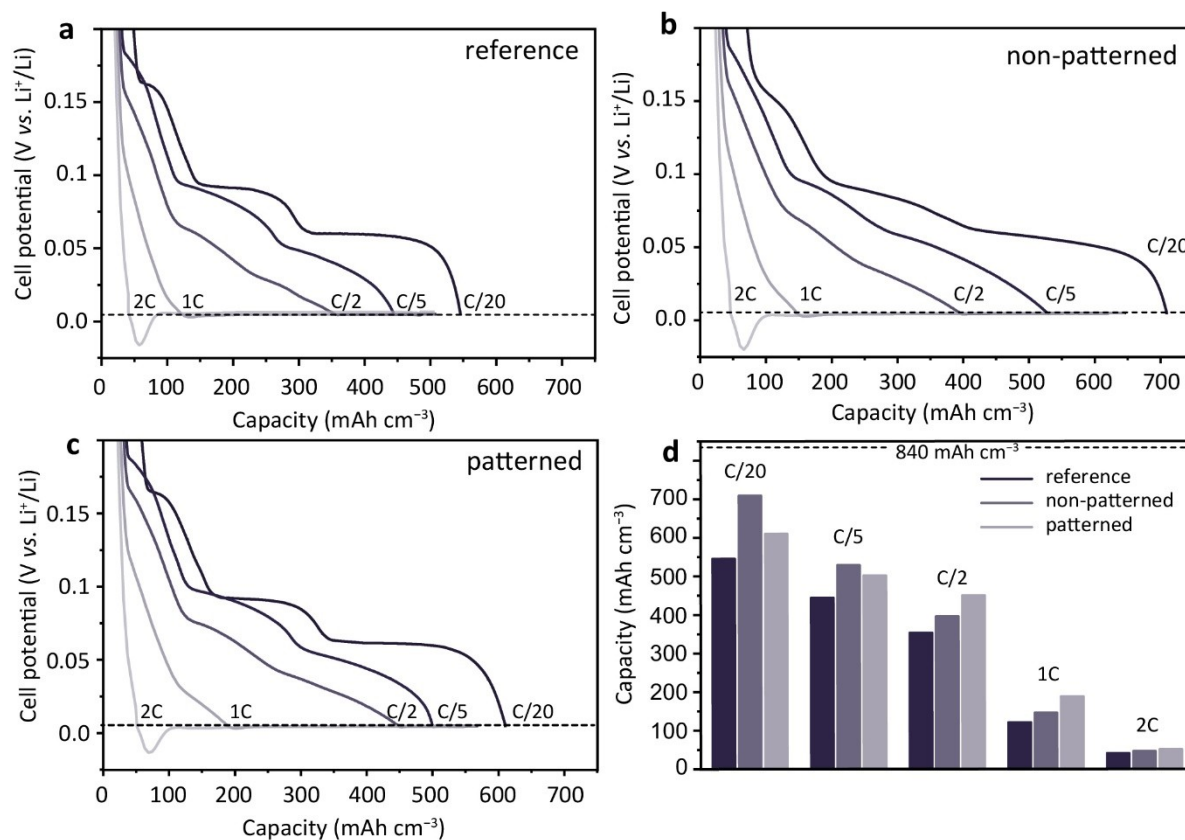

Figure 3. Constant current-constant voltage discharge profiles of a) reference, b) non-patterned and c) patterned electrodes and d) their corresponding galvanostatic capacities measured at different C rates of C/5 (2nd cycle), C/2 (7th cycle), 1C (12th cycle) and 2C (17th cycle). The gravimetric voltage profiles of studied graphite electrodes are shown in Figure S3. The dependence of gravimetric charge storage capacity vs. cycle number is shown in Figure S4.

Batteries & Supercaps

Communications
doi.org/10.1002/batt.202000253

Chemistry Europe
European Chemical
Societies Publishing

based on the theoretical work of Doyle and Newman,[24] which was simplified considering that (i) the Bruggeman dependence of the tortuosity on porosity contains a constant pre-factor γ, (ii) thickness of the separator equals zero, (iii) transference number is constant.

The total steady-state concentration drop in the patterned and non-patterned electrodes was calculated from Equations (1) and (2):

$$\Delta C_{patterned} = \left(\frac{1}{\Delta C_{CH} + \Delta C_L} + \frac{1}{\Delta C_{1D}} \right)^{-1}, \qquad (1)$$

$$\Delta C_{non-patterned} = \left(\frac{\gamma T}{2FD_0 P^{\frac{3}{2}}} \right) i, \qquad (2)$$

where ΔC_{1D} is the steady-state concentration drop in a bulk graphite electrode (in $mol\,m^{-3}$), representing Li-ion diffusion through the graphite matrix, ΔC_{CH} is the steady-state concentration drop in the vertical channel (in $mol\,m^{-3}$), representing Li-ion diffusion along channels, ΔC_L is the steady-state concentration drop that corresponds to the radial diffusion of Li^+ ions from the channel to the matrix (in $mol\,m^{-3}$), P is the electrode porosity (set to the range of 0 to 1, where 0 corresponds to the porosity in a fully dense matrix), γ is the Bruggeman pre-factor, T is the electrode thickness (in m), F is the Faraday constant (96 485.3329 $A\,s\,mol^{-1}$), D_0 is the diffusion coefficient in the electrolyte (in $m^2\,s^{-1}$), i is the current density (in $A\,m^{-2}$). It should be noted that the equation (2) is valid as long as $i < i_L$, where i_L is the limiting current density at which the percolating of Li^+ ions in the pores of the electrode becomes a limiting factor as compared to, for instance, the percolation of electrons within the electrode. The corresponding equations for concentration drops ΔC_{1D}, ΔC_{CH}, ΔC_L, limiting current density i_L, the electrode porosity P and all other constant parameters used in the simulations can be found in the Supporting Information (see Equations S1–S7 and Table S1). The general drawing of patterned electrode visualizing steady-state concentration drops ΔC_{1D}, ΔC_{CH} and ΔC_L is shown in Figure S7.

The simulation results of total steady-state concentration drop in reference, non-patterned and patterned electrodes are summarized in Figure 4. The results reveal that steady-state concentration drops at C/20 rate are very small in the range of 20–75 $mol\,m^{-3}$ for all three electrodes. At such low current density, the volumetric charge storage capacity of graphite electrodes is not limited by the Li-ion diffusion across the electrode but by their overall density. Consequently, the highest volumetric capacity at C/20 was observed for a highly dense non-patterned electrode as compared to patterned and reference electrodes of lower overall density. However, at 1C rate, a large drop of total steady-state concentration for all three electrodes indicates that Li-ion diffusion becomes the limiting factor. Therefore, the overall volumetric capacity of patterned electrodes is higher at 1C rate than for non-patterned electrodes due to a significant decrease of through-plane tortuosity and lower steady-state concentration drop owing to the presence of vertically aligned microchannels.
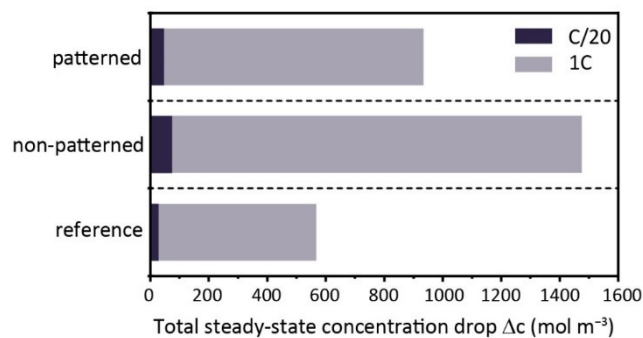

Figure 4. Total steady-state concentration drops Δc for reference, non-patterned and patterned electrodes at C/20 and 1C rates, corresponding to the current densities of 0.45 $mA\,cm^{-2}$ and 4.5 $mA\,cm^{-2}$, accordingly.

Interestingly, the further reduction of the spacing between the channels could potentially result in a lower concentration drop, leading to even higher volumetric capacities at higher current densities (Figure S8). It should be noted that although the reference electrode was characterized by a minimal total steady-state concentration drop at 1C rate, it eventually delivered the lowest volumetric capacity compared to non-patterned and patterned electrodes, owing to its very high porosity of 32%.

In summary, we report the assessment of laser patterning as a compelling methodology to boost Li-ion diffusion within compressed high areal capacity graphite electrodes (4.5 $mAh\,cm^{-2}$) through the fabrication of periodically aligned vertical microchannels. Patterned electrodes exhibited enhanced rate capability, delivering a high volumetric capacity of 450 $mAh\,cm^{-3}$ at C/2 rate as compared to the non-patterned electrode. The improvement of electrochemical performance through laser patterning is a result of a significant decrease of through-plane tortuosity, and consequently, the reduction of total steady-state concentration drop within the graphite electrodes at high current densities.

Acknowledgements

Conflict of Interest

The authors declare no conflict of interest.

[1] R. Schmuch, R. Wagner, G. Hörpel, T. Placke, M. Winter, *Nat. Energy* **2018**, *3*, 267–278.

[2] X.-G. Yang, C.-Y. Wang, *J. Power Sources* **2018**, *402*, 489–498.

[3] A. S. Mussa, A. Liivat, F. Marzano, M. Klett, B. Philippe, C. Tengstedt, G. Lindbergh, K. Edström, R. W. Lindström, P. Svens, *J. Power Sources* **2019**, *422*, 175–184.

[4] K. G. Gallagher, S. E. Trask, C. Bauer, T. Woehrle, S. F. Lux, M. Tschech, P. Lamp, B. J. Polzin, S. Ha, B. Long, Q. Wu, W. Lu, D. W. Dees, A. N. Jansen, *J. Electrochem. Soc.* **2015**, *163*, A138-A149.

[5] K.-H. Chen, K. N. Wood, E. Kazyak, W. S. LePage, A. L. Davis, A. J. Sanchez, N. P. Dasgupta, *J. Mater. Chem. A* **2017**, *5*, 11671–11681.

[6] K. N. Wood, E. Kazyak, A. F. Chadwick, K.-H. Chen, J.-G. Zhang, K. Thornton, N. P. Dasgupta, *ACS Cent. Sci.* **2016**, *2*, 790–801.

[7] K. N. Wood, M. Noked, N. P. Dasgupta, *ACS Energy Lett.* **2017**, *2*, 664–672.

[8] C.-J. Bae, C. K. Erdonmez, J. W. Halloran, Y.-M. Chiang, *Adv. Mater.* **2013**, *25*, 1254–1258.

[9] W. Pfleging, J. Pröll, *J. Mater. Chem. A* **2014**, *2*, 14918–14926.

[10] J. Pröll, H. Kim, A. Piqué, H. J. Seifert, W. Pfleging, *J. Power Sources* **2014**, *255*, 116–124.

[11] M. O. J. Ebner, PhD thesis, ETH-Zürich (Switzerland), **2014**.

[12] L. Li, R. M. Erb, J. Wang, J. Wang, Y.-M. Chiang, *Adv. Energy Mater.* **2019**, *9*, 1802472.

[13] J. S. Sander, R. M. Erb, L. Li, A. Gurijala, Y. M. Chiang, *Nat. Energy* **2016**, *1*, 16099.

[14] J. Billaud, F. Bouville, T. Magrini, C. Villevieille, A. R. Studart, *Nat. Energy* **2016**, *1*, 16097.

[15] K.-H. Chen, M. J. Namkoong, V. Goel, C. Yang, S. Kazemiabnavi, S. M. Mortuza, E. Kazyak, J. Mazumder, K. Thornton, J. Sakamoto, N. P. Dasgupta, *J. Power Sources* **2020**, *471*, 228475.

[16] L. Kraft, J. B. Habedank, A. Frank, A. Rheinfeld, A. Jossen, *J. Electrochem. Soc.* **2019**, *167*, 013506.

[17] J. B. Habedank, L. Kraft, A. Rheinfeld, C. Krezdorn, A. Jossen, M. F. Zaeh, *J. Electrochem. Soc.* **2018**, *165*, A1563-A1573.

[18] P. Smyrek, J. Pröll, H. J. Seifert, W. Pfleging, *J. Electrochem. Soc.* **2015**, *163*, A19-A26.

[19] M. Mangang, H. J. Seifert, W. Pfleging, *J. Power Sources* **2016**, *304*, 24–32.

[20] W. Pfleging, *Nat. Photonics* **2018**, *7*, 549.

[21] P. Novák, W. Scheifele, M. Winter, O. Haas, *J. Power Sources* **1997**, *68*, 267–270.

[22] J. S. Bridel, T. Azaïs, M. Morcrette, J. M. Tarascon, D. Larcher, *J. Electrochem. Soc.* **2011**, *158*, A750.

[23] M. Winter, J. O. Besenhard, M. E. Spahr, P. Novák, *Adv. Mater.* **1998**, *10*, 725–763.

[24] M. Doyle, J. Newman, *J. Appl. Electrochem.* **1997**, *27*, 846–856.